Available online at www.sciencedirect.com
SCIENCE DIRECT®
ELSEVIER
Applied Numerical Mathematics 51 (2004) 187–205
APPLIED NUMERICAL MATHEMATICS
www.elsevier.com/locate/apnum

Geometrical image segmentation by the Allen–Cahn equation

Michal Beneš [a,*], Vladimír Chalupecký [a], Karol Mikula [b]

[a] *Department of Mathematics, Faculty of Nuclear Sciences and Physical Engineering, Czech Technical University of Prague, Trojanova 13, 120 00 Prague, Czech Republic*
[b] *Department of Mathematics and Descriptive Geometry, Slovak University of Technology, Radlinského 11, 813 68 Bratislava, Slovakia*

Available online 5 June 2004

Abstract

We present an algorithm of pattern recovery (image segmentation) based on the solution of the Allen–Cahn equation. The approach is usually understood as a regularization of the level-set motion by mean curvature where we impose a special forcing term which lets the initial level set closely surround the pattern in question. We show convergence of the numerical scheme and demonstrate function of the algorithm on several artificial as well as real examples.

Keywords: Image segmentation; Allen–Cahn equation; Finite-difference method; Mean curvature flow

1. Introduction

The level set technique is known in the image-processing community due to its successful applicability, e.g., to filtering and segmentation tasks (see [14]). In this paper, we suggest an alternative based on the phase-field approach to the mean-curvature flow (see [16,6]). The phase-field methods are used in a wide range of problems (e.g., differential geometry, phase transitions) as discussed in [36,4]. We offer a new application of such methods to the rapidly growing domain of image processing by PDEs (see [13,14]).

In particular, we propose an algorithm for image segmentation, i.e., a technique devoted to recovery of pattern boundaries from the original, possibly noisy image or signal. The algorithm is based on numerical solution of the generalized Allen–Cahn equation which is a nonlinear parabolic partial differential

* Corresponding author.
E-mail addresses: michal.benes@fjfi.cvut.cz (M. Beneš), chalupec@bimbo.fjfi.cvut.cz (V. Chalupecký), mikula@ops.svf.stuba.sk (K. Mikula).

0168-9274/$30.00
doi:10.1016/j.apnum.2004.05.001

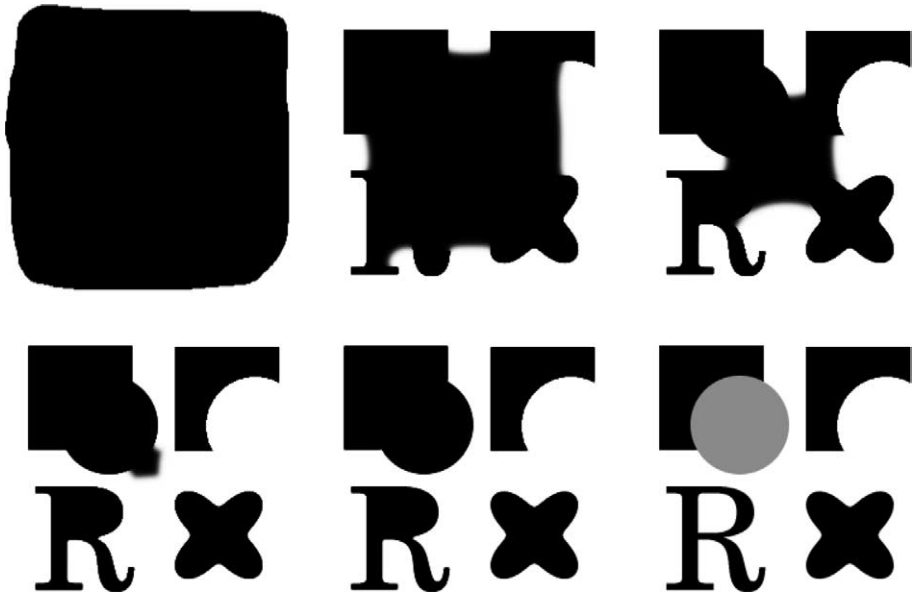

Fig. 1. Image size: 256 by 256 pixels, parameters: $h = 0.04$, $\tau = 0.001$, $\xi = 0.05$, $F = 15$, $\lambda = 10$. The time steps 0, 100, 200, 300 and 835 are shown. The original image is in the bottom right corner.

equation arising in the treatment of mean-curvature flow problems. This modification is new among the phase-field models. We show the convergence of the discrete solution given by the proposed fully discrete scheme to the weak solution. Our segmentation equation has the following form:

$$\xi \frac{\partial p}{\partial t} = \xi \nabla \cdot \big(g\big(|\nabla G_\sigma * P_0|\big)\nabla p\big) + g\big(|\nabla G_\sigma * P_0|\big)\bigg(\frac{1}{\xi} f_0(p) + \xi F|\nabla p|\bigg). \tag{1}$$

The image is located in a rectangular two-dimensional domain Ω. The segmentation process is parametrized by the variable t playing the role of time in the physical context. The function $p = p(t, x)$ should bring the initial segmentation (phase) function p_{ini} as close as possible to objects in the target (the original image P_0) in certain sense.

The initial guess p_{ini} can be given in the form of the characteristic function of the domain covering the objects of interest (see Figs. 1–4, 7) or as the characteristic function of a growing initial seed inside the object of interest (see Figs. 5, 6). At any time moment we can detect the level set $p = \frac{1}{2}$ as a segmentation curve which is moving towards edges in the image P_0.

The equation uses a non-increasing Perona–Malik function $g : \mathbb{R}_0^+ \to \mathbb{R}^+$ (compare with [32]), for which $g(0) > 0$, $g(s) \to 0$ for $s \to \infty$, and $g(\sqrt{s})$ is smooth. The function g is combined with a smoothing kernel $G_\sigma \in C^\infty(\mathbb{R}^2)$ usually represented by the Gauss function or a mollifier with compact support [10,22] satisfying

$$\int_{\mathbb{R}^2} G_\sigma(x)\,\mathrm{d}x = 1, \quad \int_{\mathbb{R}^2} |\nabla G_\sigma|\,\mathrm{d}x \leqslant C_\sigma,$$

$G_\sigma(x) \to \delta_x$ for $\sigma \to 0$, δ_x is the Dirac function at point x.

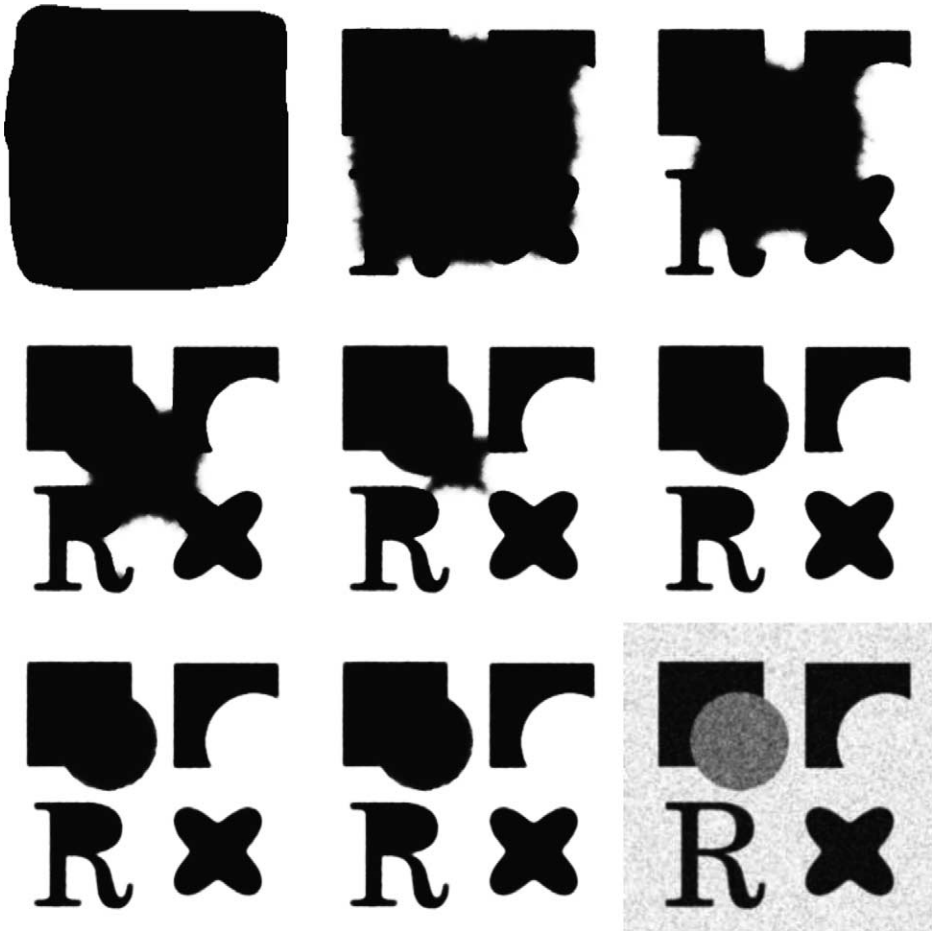

Fig. 2. Image size: 256 by 256 pixels, parameters: $h = 0.04$, $\tau = 0.001$, $\xi = 0.05$, $F = 15$, $\lambda = 10$. The time steps 0, 200, 400, 600, 800, 1000, 1400, 1765 are shown. The original image is in the bottom right corner.

The equation also contains the function f_0 and the parameters ξ, F, which are given below together with the complete setting of the initial-boundary-value problem.

The role of convolution with a smoothing kernel is to change a piecewise constant digital image (given discretely) to the infinitely smooth function for which differential quantities, e.g., gradients, are well defined. At the same time the convolution is used in pre-filtering the image P_0 before segmentation in order to smooth spurious structures like noise.

In our work we are motivated by the results related to the geodesic (or conformal) mean-curvature motion of planar curves [23,9] in the level-set formulation described by the equation

$$\begin{aligned}\frac{\partial p}{\partial t} &= |\nabla p| \nabla \cdot \left(g\big(|\nabla G_\sigma * P_0|\big) \frac{\nabla p}{|\nabla p|} \right) \\ &= |\nabla p| \left(g\big(|\nabla G_\sigma * P_0|\big) \nabla \cdot \frac{\nabla p}{|\nabla p|} + \nabla g\big(|\nabla G_\sigma * P_0|\big) \cdot \frac{\nabla p}{|\nabla p|} \right). \end{aligned} \tag{2}$$

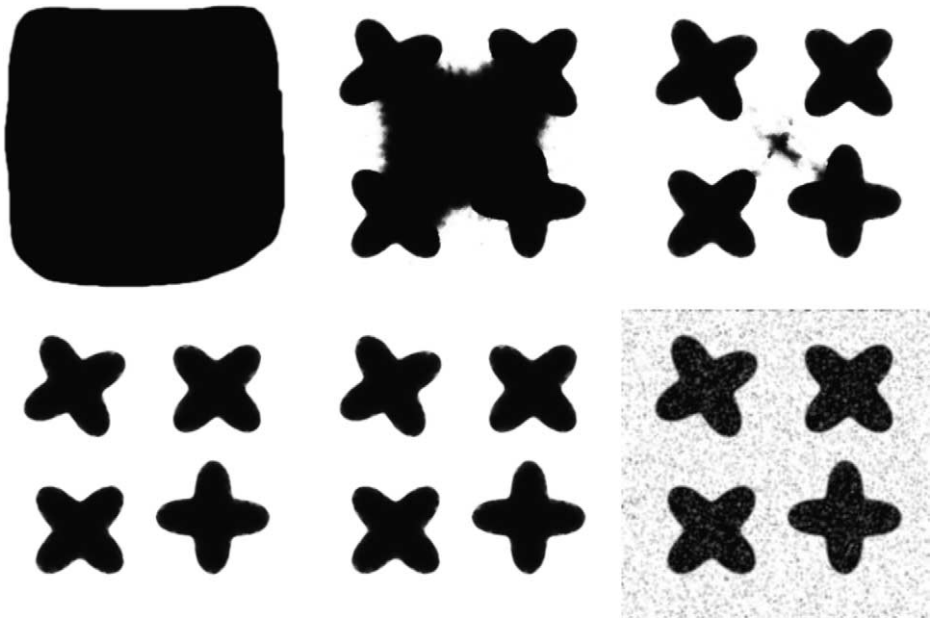

Fig. 3. Image size: 256 by 256 pixels, parameters: $h = 0.04$, $\tau = 0.0006$, $\xi = 0.05$, $F = 20$, $\lambda = 5$. The time steps 0, 100, 200, 300, 400, 532 are shown. The original image is in the bottom right corner.

The segmentation model (2) is an important generalization of the level-set equation (see [35])

$$\frac{\partial p}{\partial t} = |\nabla p| \nabla \cdot \frac{\nabla p}{|\nabla p|}, \tag{3}$$

used in a wide range of applications (see [35,29]). The curvature-driven level-set equation (3) and its various generalizations arise in two main contexts of image processing: in filtering and in segmentation.

In case of *image filtering* the function $p(t, x)$ represents an updated intensity function starting at the original image P_0 (i.e., we set $p_{\text{ini}} = P_0$). According to Eq. (3) each level line of the image intensity p moves with normal velocity proportional to its curvature. For example, the mean-curvature motion without external forcing shrinks any closed curve to a point with asymptotically infinite speed (see, e.g., [27]). Noise (a small structure with high curvature) disappears relatively fast as a consequence of such evolution. This fact may justify the use of level-set-like equations in image filtering. Edge information can also be incorporated into such models. The Perona–Malik idea of a controlled, selective diffusion is adopted here. For example, in [1], the mean-curvature motion is modified according to the following equation

$$\frac{\partial p}{\partial t} = g\big(|\nabla G_\sigma * p|\big)|\nabla p| \nabla \cdot \frac{\nabla p}{|\nabla p|}, \tag{4}$$

where the edge-indicator term g is dynamically updated following the diffused image. The term $g(|\nabla G_\sigma * p|)$ is used to slow down the motion of image contours (edges). Noise in the regions between edges is removed by the mean-curvature flow. Numerical methods solving this equation and applications in image filtering have been discussed in [1,12].

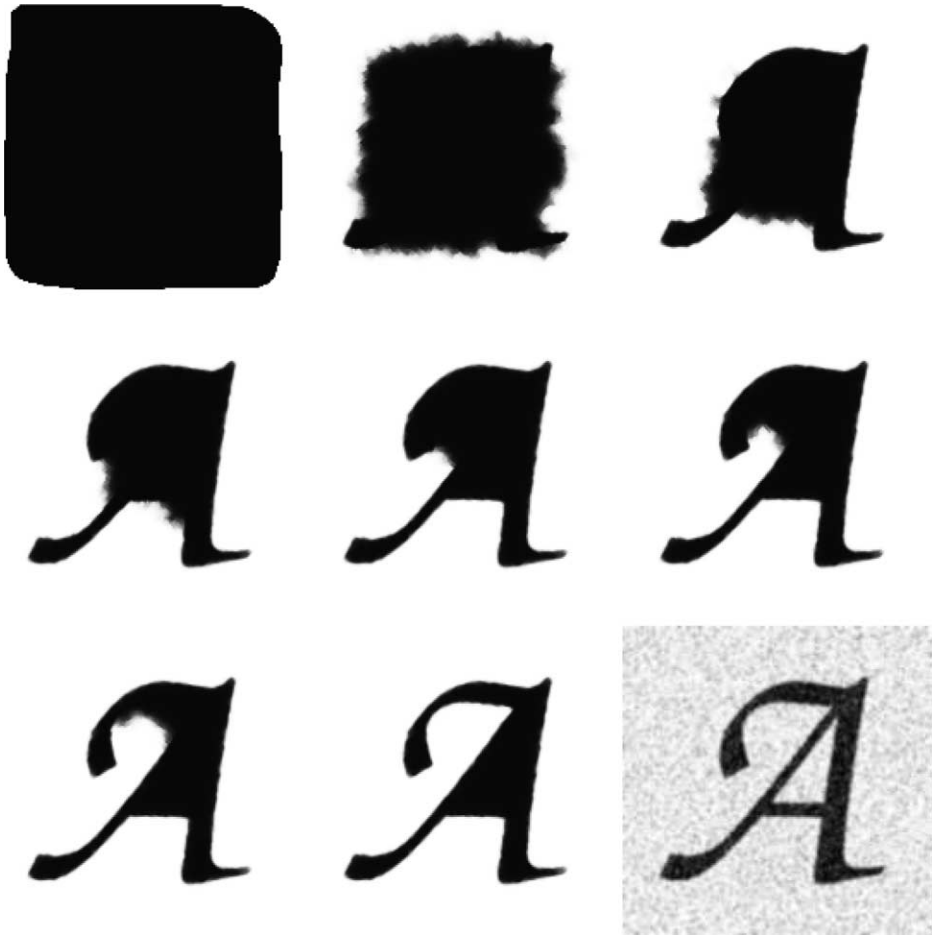

Fig. 4. Image size: 180 by 180 pixels, parameters: $h = 0.05$, $\tau = 0.001$, $\xi = 0.05$, $F = 10$, $\lambda = 20$. The time steps 0, 1000, 2000, 3000, 4000, 5000, 6000, 7371 are shown. The original image is in the bottom right corner.

Partial differential equations for *image segmentation* are similar to (4). However, as mentioned above, the sense of the solution p is different. The equation

$$\frac{\partial p}{\partial t} = g\big(|\nabla G_\sigma * P_0|\big)|\nabla p|\left(\nabla \cdot \frac{\nabla p}{|\nabla p|} + F\right), \tag{5}$$

has been proposed for the two- and three-dimensional pattern recognition (see [9,26]). In this case, $p(t, x)$ is the segmentation function whose particular level set evolves to the edge of objects in P_0. The initial segmentation level set is put inside or outside the object. Then it is evolved in the normal direction by a constant speed F plus the curvature regularization term $\nabla \cdot \frac{\nabla p}{|\nabla p|}$ both weighted by $g(|\nabla G_\sigma * P_0|)$ representing a "distance" from the edge. However, with a nonzero F, it is not easy to guarantee that the level-set motion stops appropriately, especially in case of noisy P_0.

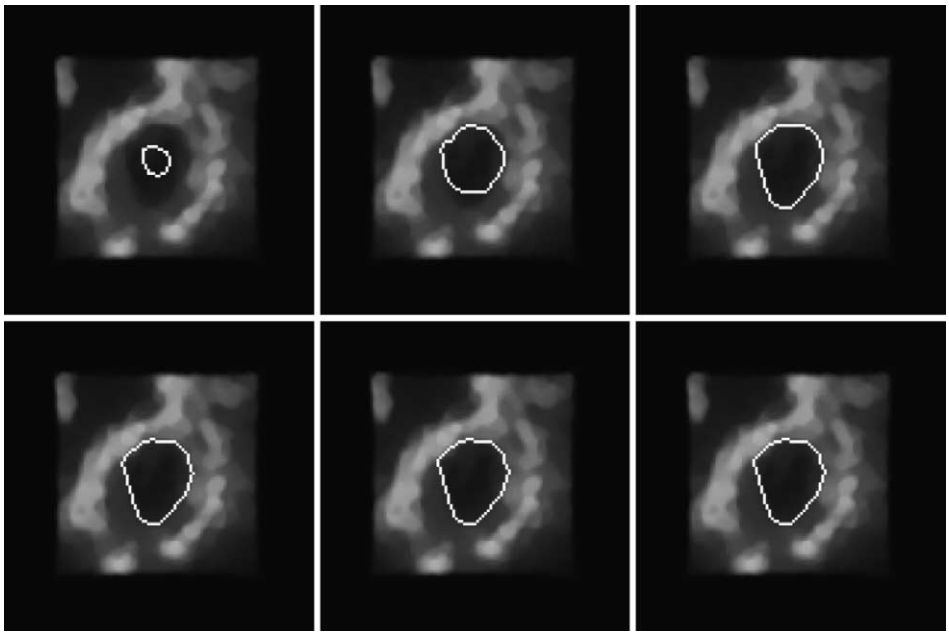

Fig. 5. Image size: 117 by 117 pixels, parameters: $h = 0.04$, $\tau = 0.001$, $\xi = 0.05$, $F = -5$, $\lambda = 10$. The time steps 0, 100, 200, 300, 400, 480 are shown.

In (2), a new driving force $-\nabla g(|\nabla G_\sigma * P_0|)$ advects the segmentation function p towards the edge. In the vicinity of an edge, the segmentation level curve is therefore automatically driven to the desired object boundary [23,9].

In this paper, we take advantage of both driving forces mentioned above. The constant one allows to bring the segmentation level curve close to the object boundary. If the segmentation curve is expected to shrink from outside the object to its edges, then $F > 0$. If the segmentation curve is to expand from the interior of the object towards the object edges, then $F < 0$. The vector field $-\nabla g(|\nabla G_\sigma * P_0|)$ allows to accurately detect the edges. The curvature regularization term makes the final curve smooth and causes minimization of the curve length in regions with missing edge information (e.g., due to noise). Furthermore, we propose the model which replaces the level-set formulation by the phase-field technique (see, e.g., [8,3]). A series of results is known, which shows a correspondence between the two approaches within the context of mean-curvature flow (see, e.g., [16]) and within the context of phase transitions (see [17,3,24]). We show that the resulting modified Allen–Cahn equation can be solved numerically without any difficulties and that corresponding numerical algorithm can be used in the above-described image-processing operations.

We organize our text as follows. In Section 2, we present known results concerning our problem, we propose the nonlinear fully-discrete semi-implicit finite-difference scheme for the numerical solution. The scheme leads to the solution of a nonlinear algebraic system at each discrete time level. Here, the nonlinear Gauss–Seidel iteration technique is used. In Section 3, we prove the convergence of the fully discrete scheme to the weak solution of our problem. In Section 4, numerical examples of image segmentation in both artificial and real images are discussed.

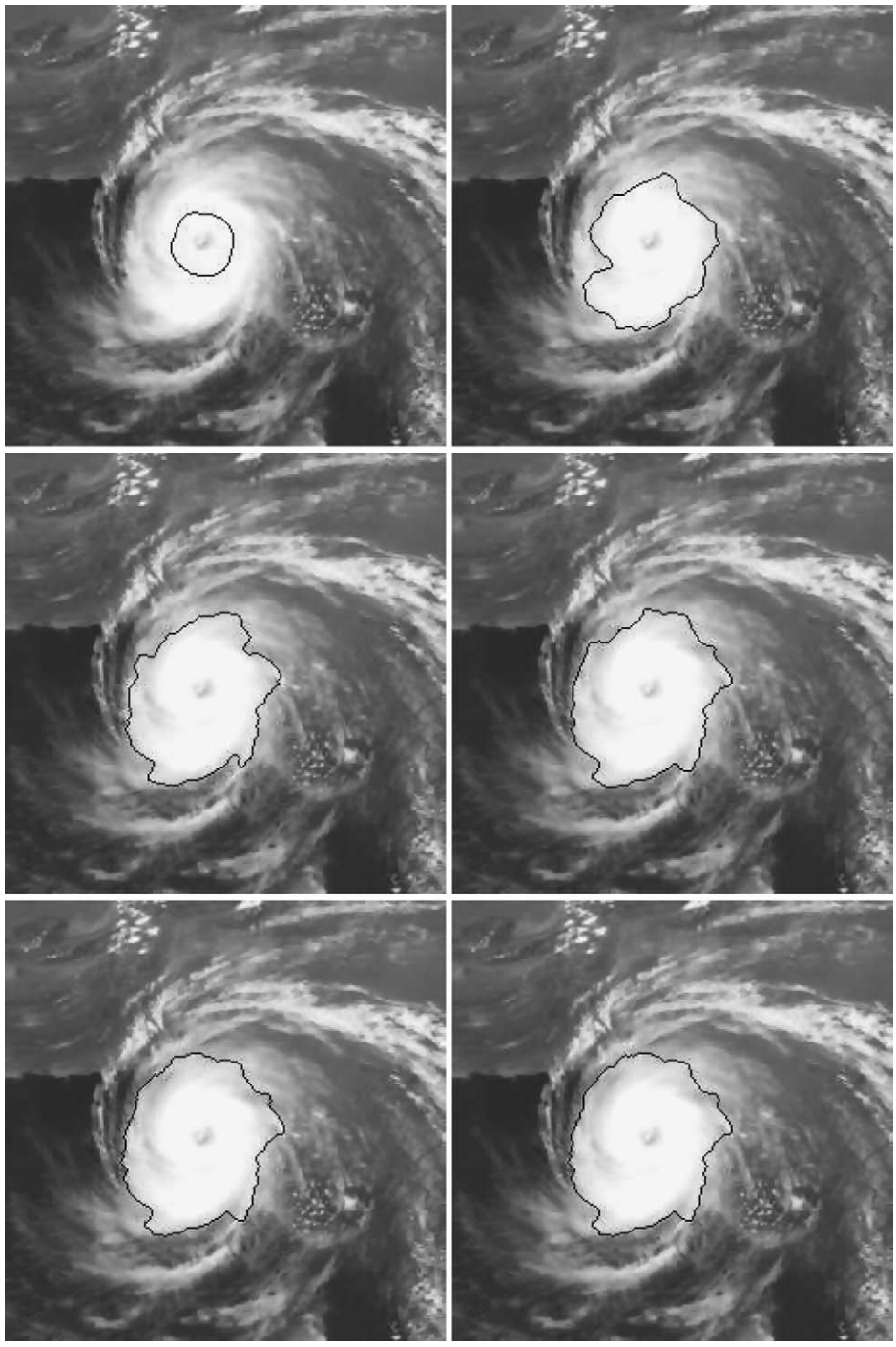

Fig. 6. Image size: 250 by 250 pixels, parameters: $h = 0.04$, $\tau = 0.0009$, $\xi = 0.06$, $F = -5$, $\lambda = 50$. The time steps 0, 1000, 2000, 3000, 4000, 4329 are shown.

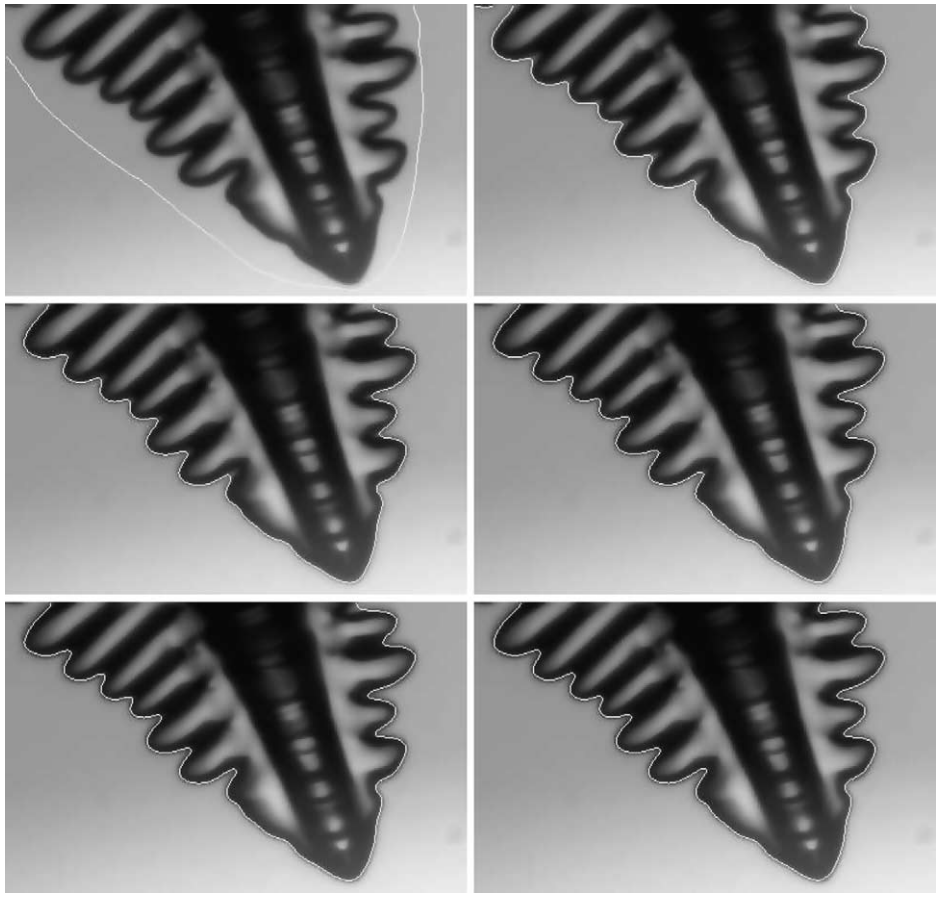

Fig. 7. Image size: 252 by 400 pixels, parameters: $h = 0.04$, $\tau = 0.001$, $\xi = 0.05$, $F = 15$, $\lambda = 40$. The time steps 0, 500, 1000, 1500, 2000, 2660 are shown.

2. Modified Allen–Cahn equation

We recall and study in detail an initial-boundary-value problem for the parabolic semi-linear partial differential equation (1) which is of the Allen–Cahn type. For this purpose we denote the rectangular domain $\Omega = (0, L_1) \times (0, L_2) \subset \mathbb{R}^2$, $x = [x_1, x_2] \in \Omega$, the time variable $t \in (0, T)$. The problem for the unknown function $p = p(t, x)$ reads as follows

$$\xi \frac{\partial p}{\partial t} = \xi \nabla \cdot \big(g\big(|\nabla G_\sigma * P_0|\big)\nabla p\big) + g\big(|\nabla G_\sigma * P_0|\big)\left(\frac{1}{\xi} f_0(p) + \xi F |\nabla p|\right) \quad \text{in } (0, T) \times \Omega,$$
$$\left.\frac{\partial p}{\partial n}\right|_{\partial\Omega} = 0 \quad \text{on } (0, T) \times \partial\Omega, \ p|_{t=0} = p_{\text{ini}}(x) \text{ in } \overline{\Omega}. \tag{6}$$

Here, $\xi > 0$ is a parameter related to the thickness of the interface layer (it is usually set to a value $\ll 1$). The polynomial $f_0(p) = ap(1-p)(p-\frac{1}{2})$, with $a > 0$, is derived from the double-well potential w_0 as $w_0' = -f_0$. The function $F = F(x)$ is bounded and continuous, the function $g \in \mathcal{C}^\infty$ strictly positive. The

function p_{ini} is the initial condition, the function $P_0 \in \mathrm{L}_\infty(\Omega)$. We refer the reader to [4,3] for details concerning the equation and physical background of it.

We observe that the function $g(|\nabla G_\sigma * P_0|)$ is infinitely smooth and bounded. We will denote it $g = g(x)$ again and we stress the following properties

$$0 < \gamma_1 \leqslant g(x) \leqslant \gamma_2, \quad \forall x \in \Omega, \tag{7}$$

where γ_1, γ_2 are positive constants.

Remark. A minor modification in the proof of Theorem 3.2 in [3] yields the existence and uniqueness of the weak solution of (6) provided $\Omega \subset \mathbb{R}^2$ is a bounded rectangular domain and $p_{\mathrm{ini}} \in \mathrm{H}^1(\Omega)$. We also see that $p \in \mathrm{L}_2(0, T; \mathrm{H}^2(\Omega))$. We notice that the numerical analysis presented below will confirm the existence result implicitly.

In case that $g = 1$, the problem (6) can be studied within the context of the mean-curvature flow (see [18,11] for the introduction, [2,6] for the current context). When $\xi \to 0_+$, the motion law $v_\Gamma = -\kappa_\Gamma - F$ is recovered with the accuracy up to the order of ξ^2 in terms of formal asymptotic expansion (see [3, Lemma 4.6]). Here, v_Γ denotes the normal velocity and κ_Γ the mean curvature of the level set $\Gamma \equiv p = \frac{1}{2}$. More details concerning the asymptotic behaviour of the problem (6) when $\xi \to 0_+$ can be found, e.g., in Theorem 2.2 of [6].

Numerical scheme

A discretized version of the problem (6) will be used in the context of image processing. We propose the numerical scheme based on the finite-difference method in space and time. First, we summarize some notation of the spatial discretization—h_1, h_2 are the mesh sizes, $\omega_h = \{[ih_1, jh_2] \mid i = 1, \ldots, N_1 - 1;\ \ j = 1, \ldots, N_2 - 1\}$, $\bar{\omega}_h = \{[ih_1, jh_2] \mid i = 0, \ldots, N_1;\ \ j = 0, \ldots, N_2\}$ grids of internal and of all nodes, respectively, $u_{\bar{x}_1}$, $u_{\bar{x}_2}$ backward differences, u_{x_1}, u_{x_2} forward differences, $\bar{\nabla}_h u = [u_{\bar{x}_1}, u_{\bar{x}_2}]$ and $\nabla_h u = [u_{x_1}, u_{x_2}]$ (details can be found in [6]). Introducing the time step $\tau > 0$, the time-level index is $k = 0, 1, \ldots, N_T$. We can consider the grid function $v : \{0, 1, \ldots, N_T\} \times \bar{\omega}_h \to \mathbb{R}$ for which $v_{ij}^k = v(k\tau, ih_1, jh_2)$, $\delta v_{ij}^k = \frac{v_{ij}^k - v_{ij}^{k-1}}{\tau}$. We also introduce a linear space of grid functions with homogeneous discrete Neumann conditions $\mathcal{H}_h = \{u : \bar{\omega}_h \to \mathbb{R} \mid u_{x_1,0j} = 0,\ \ u_{x_2,i0} = 0,\ \ u_{\bar{x}_1,N_1 j} = 0,\ u_{\bar{x}_2,iN_2} = 0,\ \ i = 0, \ldots, N_1,\ \ j = 0, \ldots, N_2\}$. We propose the two-level semi-implicit finite-difference scheme in the following form at the time level k

$$\begin{aligned} &\xi \delta p_h^k = \xi \nabla_h \cdot \left(g \bar{\nabla}_h p_h^k\right) + g\left(\frac{1}{\xi} f_0\left(p_h^k\right) + \xi F\left|\bar{\nabla}_h p_h^{k-1}\right|\right) \quad \text{on } \omega_h, \\ &p_h^k \in \mathcal{H}_h,\ \ p_h^0 = \mathcal{P}_h p_{\mathrm{ini}}, \end{aligned} \tag{8}$$

where the solution is a map $p_h : \{1, \ldots, N_T\} \times \bar{\omega}_h \to \mathbb{R}$, g stands for the grid values of the function $g(x)$ (see Section 4) and $\mathcal{P}_h : \mathcal{C}(\overline{\Omega}) \to \mathcal{H}_h$ is the projection (restriction) operator. We observe that the scheme (8) is nonlinear with respect to p_h^k and dominated by the second-order difference operator. The convergence result is contained in the following statement:

Theorem 1. *The scheme* (8) *has the unique solution for τ small. If $\tau \to 0_+$ and $h \to 0_+$, then this solution converges to the weak solution of* (6) *provided* $p_{\mathrm{ini}} \in \mathrm{H}^1(\Omega) \cap \mathcal{C}(\overline{\Omega})$.

3. Convergence of the numerical scheme

Finite-difference interpolation theory

In this section, we summarize features of grid functions and their interpolants. Details can be found in [6] and related references therein. We use them when proving the above mentioned result. If $f, g \in \mathcal{H}_h$, $\mathbf{f} = [f^1, f^2]$ and $\mathbf{g} = [g^1, g^2]$, we denote $(f, g)_h = \sum_{i,j=1}^{N_1-1,N_2-1} h_1 h_2 f_{ij} g_{ij}$, $\|f\|_h^2 = (f, f)_h$, $(\mathbf{f}, \mathbf{g}] = \sum_{i=1,j=1}^{N_1,N_2-1} h_1 h_2 f_{ij}^1 g_{ij}^1 + \sum_{i=1,j=1}^{N_1-1,N_2} h_1 h_2 f_{ij}^2 g_{ij}^2$, $\|\mathbf{f}]|^2 = (\mathbf{f}, \mathbf{f}]$. According to [33], the discrete analogues of various integral relations are valid, in particular the Green formula for $f, g \in \mathcal{H}_h$ and $p : \bar{\omega}_h \to \mathbb{R}$: $(f, \nabla_h(p\bar{\nabla}_h g)_h) = -(p\bar{\nabla}_h f, \bar{\nabla}_h g]$. We continue by introducing extensions of grid functions, so that they are defined almost everywhere on Ω. Such extensions are studied by the usual technique of Lebesgue and Sobolev spaces.

Remark. We recall necessary definitions needed to extrapolate grid functions in $\mathbb{R}^2$ (see [6]). We also define a subdomain $\Omega_h \subset \Omega$ consisting of thin bands near $\partial\Omega$:

$$\Omega_h = (0, L_1) \times (0, h_2/2) \cup (0, L_1) \times (N_2 - h_2/2, N_2) \cup (0, h_1/2) \times (0, L_2) \cup (N_1 - h_1/2, N_1) \times (0, L_2).$$

We use the *piecewise linear interpolation* operator $\mathcal{Q}_h : \mathcal{H}_h \to \mathcal{C}(\overline{\Omega})$ defined in the usual way (see [7]) on the triangles given by the grid $\bar{\omega}_h$ with diagonals connecting the nodes $(i-1, j)$ and $(i, j-1)$. The *piecewise constant interpolation* operator $\mathcal{S}_h : \mathcal{H}_h \to \mathrm{L}_\infty(\Omega)$ is built on rectangular cells centered on the nodes of ω_h ($\mathcal{S}_h u = 0$ on Ω_h). The *piecewise constant interpolation* operator $\widetilde{\mathcal{S}}_h : \mathcal{H}_h \to \mathrm{L}_\infty(\Omega)$ is built on rectangular cells centered on the nodes of $\bar{\omega}_h$. We proceed by determining basic properties of the above defined maps as implied by [6] and by the references therein:

(1) If $u, v \in \mathcal{H}_h$, then $\int_\Omega \mathcal{S}_h u \mathcal{S}_h v \,\mathrm{d}x = (u, v)_h$.
(2) If $u, v \in \mathcal{H}_h$, then

$$\int_\Omega \widetilde{\mathcal{S}}_h u \widetilde{\mathcal{S}}_h v \,\mathrm{d}x = (u, v)_h + \frac{1}{2} h_1 h_2 \sum_{i=1}^{N_1-1} (uv|_{i0} + uv|_{iN_2}) + \frac{1}{2} h_1 h_2 \sum_{j=1}^{N_2-1} (uv|_{0j} + uv|_{N_1 j}) + \frac{1}{4} h_1 h_2 (uv|_{00} + uv|_{0N_2} + uv|_{N_1 0} + uv|_{N_1 N_2}).$$

(3) We observe that the operators $\mathcal{S}_h$ and $\widetilde{\mathcal{S}}_h$ have the following properties: $\|\mathcal{S}_h u\|_{\mathrm{L}_2(\Omega)} = \|u\|_h$, $\|\widetilde{\mathcal{S}}_h u\|_{\mathrm{L}_2(\Omega)} \leqslant 2\|u\|_h$. Furthermore, both operators have suitable convergence properties, namely $\|\mathcal{S}_h \mathcal{P}_h p - \widetilde{\mathcal{S}}_h \mathcal{P}_h p\|_{\mathrm{L}_2(\Omega)} \to 0$, whenever $h \to 0$ and $p \in \mathcal{C}(\overline{\Omega})$.
(4) Let $u, v \in \mathcal{H}_h$. Then

$$\big(\nabla(\mathcal{Q}_h u), \nabla(\mathcal{Q}_h v)\big) = \big(\bar{\nabla}_h u, \bar{\nabla}_h v\big] + E(u, v), \tag{9}$$

where we denote

$$E(u, v) = \frac{1}{2} \sum_{i=1}^{N_1} h_1 h_2 (u_{\bar{x}_1} v_{\bar{x}_1}|_{i,N_2} + u_{\bar{x}_1} v_{\bar{x}_1}|_{i,0}) + \frac{1}{2} \sum_{j=1}^{N_2} h_1 h_2 (u_{\bar{x}_2} v_{\bar{x}_2}|_{N_1,j} + u_{\bar{x}_2} v_{\bar{x}_2}|_{0,j}).$$

Consequently,

$$\left\|\nabla(\mathcal{Q}_h u)\right\|^2 \leqslant \frac{3}{2}\left\|\bar{\nabla}_h u\right]\right|^2. \tag{10}$$

(5) The relation between norms of the operators $\mathcal{Q}_h$ and $\mathcal{S}_h$: $\|\mathcal{Q}_h u\|_{\mathrm{L}_2(\Omega)} \leqslant 2\|\mathcal{S}_h u\|_{\mathrm{L}_2(\Omega)}$ is implied by a similar relation $\|\mathcal{Q}_h u\|_{\mathrm{L}_2(\Omega)} \leqslant \|\widetilde{\mathcal{S}}_h u\|_{\mathrm{L}_2(\Omega)}$ given in [6] and by the point 3 of this list.
(6) The convergence property $\|\mathcal{S}_h \mathcal{P}_h p - \mathcal{Q}_h \mathcal{P}_h p\|_{\mathrm{L}_2(\Omega)} \to 0$ is valid whenever $h \to 0$ and $p \in \mathcal{C}(\overline{\Omega})$ (see [6] and the point 3 of this list).

Remark. According to [21], we define the Rothe functions for the interpolation along the time axis. We denote $\mathcal{H}_\tau = \{v \mid v : (0, 1, \ldots, N_T) \to \mathbb{R}\}$ the space of grid functions with respect to time. We use *piecewise linear interpolation* by means of the operator $\mathcal{Q}_\tau : \mathcal{H}_\tau \to \mathcal{C}(\langle 0, T\rangle)$ such that for each $v \in \mathcal{H}_\tau$, $(\mathcal{Q}_\tau v)(t) = v^{k-1} + \delta v^k (t - (k-1)\tau)$ for $t \in \langle (k-1)\tau, k\tau\rangle$; and *piecewise constant interpolation* operator $\mathcal{S}_\tau : \mathcal{H}_\tau \to \mathrm{L}_\infty(0, T)$ such that for each $v \in \mathcal{H}_\tau$, $(\mathcal{S}_\tau v)(t) = v^k$ for $t \in ((k-1)\tau, k\tau\rangle$. We mention the known relationship between the Rothe functions: $\int_0^T |\mathcal{Q}_\tau v - \mathcal{S}_\tau v|^2 \,\mathrm{d}t = \frac{\tau^2}{3}\sum_{k=1}^{N_T} \tau |\delta v^k|^2$.

Remark on the solvability of (8). The space $\mathcal{H}_h$ is a finite-dimensional Hilbert space with the scalar product $(u, v)_{\mathcal{H}_h} = (\bar{\nabla}_h u, \bar{\nabla}_h v] + (u, v)_h$. The operator T given by the formula

$$\left\langle T\left(p_h^k\right), v\right\rangle := \xi\left(p_h^k, v\right)_h + \xi\left(g\bar{\nabla}_h p_h^k, \bar{\nabla}_h v\right] - \frac{1}{\xi}\left(g f_0\left(p_h^k\right), v\right)_h,$$

which appears in (8), is the variation of the potential

$$\mathcal{F}(u) := \frac{\xi}{2}(u, u)_h + \frac{\xi}{2}\left(g\bar{\nabla}_h u, \bar{\nabla}_h u\right] + \frac{1}{\xi}\left(g w_0(u), 1\right)_h.$$

The function w_0, with $w_0' = -f_0$, is a double-well potential density (see [4]). The operator T on $\mathcal{H}_h$ becomes strongly monotone, following the estimate

$$\begin{aligned}\left\langle T(u) - T(v), u - v\right\rangle &= \frac{\xi}{2}\|u - v\|_h^2 + \frac{\xi}{2}\left(g\bar{\nabla}_h(u - v), \bar{\nabla}_h(u - v)\right] - \frac{\tau}{\xi}\left(g\left(f_0(u) - f_0(v)\right), u - v\right)_h \\ &\geqslant \left(\frac{\xi}{2} - \frac{\tau}{\xi}\frac{5}{8}a\gamma_2\right)\|u - v\|_h^2 + \gamma_1\frac{\xi}{2}\left\|\bar{\nabla}_h(u - v)\right]\right|^2,\end{aligned}$$

using (7), the fact that $(f_0(u) - f_0(v))(u - v) \leqslant \frac{5}{8}a(u - v)^2$ and provided the condition

$$\tau < \frac{4}{5a\gamma_2}\xi^2 \tag{11}$$

holds (in agreement with other results, e.g., [28,31]). We therefore satisfy the assumptions of [20, Theorem 26.11] and of remarks thereafter, from which we obtain existence of the unique solution of (8).

A priori estimate of the discrete solution

Now, we estimate quantities contained in the discrete scheme (8) in order to prepare the convergence proof. We multiply (8) by $\tau\delta p_h^k$, sum over ω_h and for $k = 1, \ldots, l$ and use the Green formula. Then we have

$$\xi\sum_{k=1}^{l}\tau\left\|\delta p_h^k\right\|_h^2 + \xi\sum_{k=1}^{l}\tau\left(g\bar{\nabla}_h p_h^k, \bar{\nabla}_h\delta p_h^k\right] = \frac{1}{\xi}\sum_{k=1}^{l}\tau\left(g f_0\left(p_h^k\right), \delta p_h^k\right)_h + \xi\sum_{k=1}^{l}\tau\left(g F\left|\bar{\nabla}_h p_h^{k-1}\right|, \delta p_h^k\right)_h.$$

The Abel summation rule, the relationships $|F(x)| \leqslant C_F$, and $\gamma_1 \leqslant g(x) \leqslant \gamma_2$, and a manipulation (motivated, e.g., by [34, p. 378]) with the nonlinear term $(gf_0(p_h^k), \delta p_h^k)_h$ by means of a function $h_0(s) = a(\frac{1}{2} - (s-\frac{1}{2})^2)$ such that $f_0(s) = h_0(s)(s-\frac{1}{2})$,

$$\begin{aligned}\big(gf_0\big(p_h^k\big), \delta p_h^k\big)_h &= \frac{1}{2}\left(gh_0\big(p_h^k\big)\left(\left(p_h^k - \frac{1}{2}\right) + \left(p_h^{k-1} - \frac{1}{2}\right) + \left(p_h^k - \frac{1}{2}\right) - \left(p_h^{k-1} - \frac{1}{2}\right)\right), \delta p_h^k\right)_h \\ &= -\frac{1}{4a}\delta\big(g\big|h_0\big(p_h^k\big)\big|^2, 1\big)_h - \frac{\tau}{4a}\big(g\big|\delta h_0\big(p_h^k\big)\big|^2, 1\big)_h + \frac{\tau}{2}\left(gh_0\big(p_h^k\big), \left(\delta\left(p_h^k - \frac{1}{2}\right)\right)^2\right)_h,\end{aligned}$$

allow to obtain the following inequality

$$\begin{aligned}&\xi\sum_{k=1}^{l}\tau\big\|\delta p_h^k\big\|_h^2 + \frac{\xi}{2}\sum_{k=1}^{l}\big(g\bar{\nabla}_h\big(p_h^k - p_h^{k-1}\big), \bar{\nabla}_h\big(p_h^k - p_h^{k-1}\big)\big] + \frac{\xi}{2}\big(g\bar{\nabla}_h p_h^l, \bar{\nabla}_h p_h^l\big] \\ &\quad + \frac{1}{4a\xi}\big(g\big|h_0\big(p_h^l\big)\big|^2, 1\big)_h + \frac{\tau}{4a\xi}\sum_{k=1}^{l}\tau\big(g\big|\delta h_0\big(p_h^k\big)\big|^2, 1\big)_h \\ &\leqslant \frac{\xi}{2}\big(g\bar{\nabla}_h p_h^0, \bar{\nabla}_h p_h^0\big] + \frac{1}{4a\xi}\big(g\big|h_0\big(p_h^0\big)\big|^2, 1\big)_h + \frac{\tau}{2\xi}\sum_{k=1}^{l}\tau\left(gh_0\big(p_h^k\big), \left(\delta\left(p_h^k - \frac{1}{2}\right)\right)^2\right)_h \\ &\quad + \xi C_F\gamma_2\sum_{k=1}^{l}\tau\big(\big|\bar{\nabla}_h p_h^{k-1}\big|, \delta p_h^k\big)_h.\end{aligned}$$

We treat the non-linear term as follows

$$\left(gh_0\big(p_h^k\big), \left(\delta\left(p_h^k - \frac{1}{2}\right)\right)^2\right)_h = \frac{1}{2}a\left(g\left|\delta\left(p_h^k - \frac{1}{2}\right)\right|^2, 1\right)_h - a\left(g\left(p_h^k - \frac{1}{2}\right)^2, \left|\delta\left(p_h^k - \frac{1}{2}\right)\right|^2\right)_h,$$

which together with the Young inequality applied to the term $(|\bar{\nabla}_h p_h^{k-1}|, \delta p_h^k)_h$ and by the restriction to the terms useful for our purposes gives

$$\begin{aligned}&\frac{1}{2}\xi\sum_{k=1}^{l}\tau\big\|\delta p_h^k\big\|_h^2 + \frac{\xi}{2}\gamma_1\sum_{k=1}^{l}\big(\bar{\nabla}_h\big(p_h^k - p_h^{k-1}\big), \bar{\nabla}_h\big(p_h^k - p_h^{k-1}\big)\big] \\ &\quad + \frac{\xi}{2}\gamma_1\big(\bar{\nabla}_h p_h^l, \bar{\nabla}_h p_h^l\big] + \frac{\gamma_1}{4a\xi}\big(g\big|h_0\big(p_h^l\big)\big|^2, 1\big)_h \\ &\leqslant \frac{\xi}{2}\gamma_2\big(\bar{\nabla}_h p_h^0, \bar{\nabla}_h p_h^0\big] + \frac{\gamma_2}{4a\xi}\big(g\big|h_0\big(p_h^0\big)\big|^2, 1\big)_h + \xi\gamma_2^2 C_F^2\big\|\bar{\nabla}_h p_h^0\big]\big|^2 + \xi\gamma_2^2 C_F^2\sum_{k=1}^{l}\tau\big\|\bar{\nabla}_h p_h^k\big]\big|^2.\end{aligned}$$

The discrete Gronwall lemma (see [21]) allows us to obtain that

$$\xi\big\|\bar{\nabla}_h p_h^l\big]\big|^2 \leqslant \frac{1}{(1 - 2\tau\frac{\gamma_2^2}{\gamma_1}C_F^2)^k}\left(\left(\frac{\gamma_2}{2\gamma_1} + \frac{\gamma_2^2}{\gamma_1}C_F^2\right)\xi\big\|\bar{\nabla}_h p_h^0\big]\big|^2 + \frac{\gamma_2}{4a\xi\gamma_1}\big(\big|h_0\big(p_h^0\big)\big|^2, 1\big)_h\right).$$

Assuming that p_{ini} is regular enough ($p_{\text{ini}} \in \mathrm{H}^1(\Omega) \cap C(\overline{\Omega})$), we obtain uniform boundedness of $\xi\|\bar{\nabla}_h p_h^l\|^2$, $\xi\sum_{k=1}^{l}\|\bar{\nabla}_h(p_h^k - p_h^{k-1})\|^2$, $(g|h_0(p_h^l)|^2, 1)_h$ and $\xi\sum_{k=1}^{l}\tau\|\delta p_h^k\|_h^2$ for all $l = 0, \ldots, N_T$ independently of τ, h.

Passage to the limit

We explore the interpolation operators $\mathcal{S}_h$, $\mathcal{Q}_h$ and $\mathcal{S}_\tau$, $\mathcal{Q}_\tau$. We take arbitrary sequences h_n and τ_n of space and time steps tending to 0, and look for the convergence of the approximate solutions depending on the mentioned sequences. In the following, we omit the index n. The above given properties of the mentioned operators (see also [6]) imply that $\xi\|\nabla\mathcal{S}_\tau\mathcal{Q}_h p_h^l\|^2$, $(g w_0(\mathcal{S}_\tau\mathcal{S}_h p_h^l, 1)$ and $\xi\int_0^{l\tau}\|\frac{\partial\mathcal{Q}_\tau\mathcal{S}_h p_h^k}{\partial t}\|^2$ are uniformly bounded for all $l=0,\dots,N_T$ independently of τ, h. Mutual relations of the interpolation operators listed above imply that $\mathcal{Q}_\tau\mathcal{Q}_h p_h^k$ in $\mathrm{L}_\infty(0,T;\mathrm{H}^1(\Omega))$ and $\frac{\partial\mathcal{Q}_\tau\mathcal{Q}_h p_h^k}{\partial t}$ in $\mathrm{L}_2(0,T;\mathrm{L}_2(\Omega))$ are uniformly bounded for all $k=0,\dots,N_T$ independently of τ, h. This setting is suitable for the imbedding theorem (for the given context, used, e.g., in [3]), from which we can find a subsequence strongly converging to p in $\mathrm{L}_6(0,T;\mathrm{L}_6(\Omega))$. The Aubin lemma (see [25]) as a typical argument for the given nonlinearity yields that $f_0(\mathcal{S}_\tau\mathcal{S}_h p_h^k)$ converges to $f_0(p)$ in $\mathrm{L}_2(0,T;\mathrm{L}_2(\Omega))$. Strong convergence of gradients is shown in the following lemma:

Lemma 1. *The sequence $\nabla\mathcal{S}_\tau\mathcal{Q}_h p_h^k$ converges strongly to ∇p in $\mathrm{L}_2(0,T;\mathrm{L}_2(\Omega;\mathbb{R}^2))$ and $\mathcal{S}_\tau\mathcal{S}_h|\bar\nabla_h p_h|\times(t-\tau)$ converges strongly to $|\nabla p|$ in $\mathrm{L}_2(0,T;\mathrm{L}_2(\Omega))$.*

Proof. The proof of the lemma is similar to the proof of [3, Lemma 3.4]. However, it is delivered due to points through which both proofs differ. We multiply Eq. (8) by $p_h^k-\mathcal{P}_h p$ and sum over ω_h:

$$\begin{aligned}&\xi\big(\delta p_h^k,\, p_h^k-\mathcal{P}_h p\big)_h+\xi\big(g\bar\nabla_h p_h^k,\,\bar\nabla_h\big(p_h^k-\mathcal{P}_h p\big)\big]\\&\quad=\frac{1}{\xi}\big(g f_0\big(p_h^k\big),\, p_h^k-\mathcal{P}_h p\big)_h+\xi\big(g F\big|\bar\nabla_h p_h^{k-1}\big|,\, p_h^k-\mathcal{P}_h p\big)_h.\end{aligned}$$

We add and subtract the term $\xi(g\bar\nabla_h\mathcal{P}_h p,\bar\nabla_h(p_h^k-\mathcal{P}_h p)]$ to the equality, multiply it by τ, sum over $k=1,\dots,N_T$ and rewrite in terms of Lebesgue spaces using the properties of interpolation operators

$$\begin{aligned}&\xi\int_0^T\big(\mathcal{S}_h\mathcal{P}_h g\nabla\mathcal{S}_\tau\mathcal{Q}_h\big(p_h^k-\mathcal{P}_h p\big),\nabla\mathcal{S}_\tau\mathcal{Q}_h\big(p_h^k-\mathcal{P}_h p\big)\big)\,\mathrm{d}t\\&\quad\leqslant-\xi\int_0^T\left(\frac{\partial\mathcal{Q}_\tau\mathcal{S}_h p_h^k}{\partial t},\mathcal{S}_\tau\mathcal{S}_h\big(p_h^k-\mathcal{P}_h p\big)\right)\mathrm{d}t+\frac{1}{\xi}\int_0^T\big(\mathcal{S}_h\mathcal{P}_h g f_0\big(\mathcal{S}_\tau\mathcal{S}_h p_h^k\big),\mathcal{S}_\tau\mathcal{S}_h\big(p_h^k-\mathcal{P}_h p\big)\big)\,\mathrm{d}t\\&\qquad+\xi\int_0^T\big(\mathcal{S}_h\mathcal{P}_h(gF)\mathcal{S}_\tau\mathcal{S}_h\big(\big|\bar\nabla_h p_h^{k-1}\big|\big)(t-\tau),\mathcal{S}_\tau\mathcal{S}_h\big(p_h^k-\mathcal{P}_h p\big)\big)\,\mathrm{d}t\\&\qquad-\xi\int_0^T\big(\mathcal{S}_h\mathcal{P}_h g\nabla\mathcal{S}_\tau\mathcal{Q}_h\mathcal{P}_h p,\nabla\mathcal{S}_\tau\mathcal{Q}_h\big(p_h^k-\mathcal{P}_h p\big)\big)\,\mathrm{d}t+\xi\int_0^T\mathcal{S}_\tau E\big(\mathcal{P}_h p,\,p_h^k-\mathcal{P}_h p\big)\,\mathrm{d}t.\end{aligned}$$

We observe that $\mathcal{S}_\tau\mathcal{S}_h(p_h^k-\mathcal{P}_h p)\to 0$ strongly in $\mathrm{L}_2(0,T;\mathrm{L}_2(\Omega))$, as $\mathcal{S}_\tau\mathcal{S}_h p_h^k-p\to 0$ strongly, and $\mathcal{S}_\tau\mathcal{S}_h\mathcal{P}_h p-p\to 0$ strongly in the same space due to properties of the extension operators. Furthermore, $\nabla\mathcal{S}_\tau\mathcal{Q}_h(p_h^k-\mathcal{P}_h p)\to 0$ weakly in $\mathrm{L}_2(0,T;\mathrm{L}_2(\Omega))$, as $\mathcal{Q}_\tau\mathcal{Q}_h p_h^k-p\to 0$ weakly in $\mathrm{L}_2(0,T;\mathrm{H}^1(\Omega))$,

$\mathcal{Q}_\tau \mathcal{Q}_h p_h^k - \mathcal{S}_\tau \mathcal{Q}_h p_h^k \to 0$ strongly in $\mathrm{L}_2(0,T;\mathrm{L}_2(\Omega))$. The interpolation property of $\mathcal{Q}_h$ implies that $p - \mathcal{Q}_h\mathcal{P}_h p \to 0$ in $\mathrm{H}^1(\Omega)$ (see [7]). The sequence $\int_0^T \mathcal{S}_\tau E(\mathcal{P}_h p,\, p_h^k - \mathcal{P}_h p)\,\mathrm{d}t \to 0$ as

$$\int_0^T \mathcal{S}_\tau E\big(\mathcal{P}_h p,\, p_h^k - \mathcal{P}_h p\big)\,\mathrm{d}t = \int_0^T \int_{\Omega_h} \mathcal{S}_h\mathcal{P}_h g \nabla \mathcal{S}_\tau \mathcal{Q}_h \mathcal{P}_h p \cdot \nabla \mathcal{S}_\tau \mathcal{Q}_h\big(p_h^k - \mathcal{P}_h p\big)\,\mathrm{d}x\,\mathrm{d}t,$$

and $\int_0^T\int_{\Omega_h} |\nabla \mathcal{S}_\tau \mathcal{Q}_h\mathcal{P}_h p|^2\,\mathrm{d}x\,\mathrm{d}t \leqslant 2\int_0^T\int_\Omega |\nabla \mathcal{S}_\tau \mathcal{Q}_h\mathcal{P}_h p - \nabla p|^2\,\mathrm{d}x\,\mathrm{d}t + 2\int_0^T\int_{\Omega_h} |\nabla p|^2\,\mathrm{d}x\,\mathrm{d}t$. Therefore $\nabla \mathcal{S}_\tau \mathcal{Q}_h\mathcal{P}_h p$ restricted to Ω_h tends strongly to 0, and $\nabla \mathcal{S}_\tau \mathcal{Q}_h(p_h^k - \mathcal{P}_h p)$ tends weakly to 0. As all terms in the right side tend to 0 for $n \to \infty$, we see that $\nabla(\mathcal{S}_\tau \mathcal{Q}_h(p_h^k - \mathcal{P}_h p)) \to 0$ strongly in $\mathrm{L}_2(0,T;\mathrm{L}_2(\Omega;\mathbb{R}^2))$.

Now, we use the fact that $\xi \sum_{k=1}^l \|\bar\nabla_h(p_h^k - p_h^{k-1})\|^2$ is bounded, which together with the property (9) gives the convergence of the term $\mathcal{S}_\tau\mathcal{S}_h(|\bar\nabla_h p_h^k|)(t-\tau)$ to $|\nabla p|$. □

We multiply (8) by a test function $\mathcal{P}_h w$, where $w \in \mathcal{C}_0^\infty(\Omega)$, and integrate it over ω_h. Then, we have

$$\xi\big(\delta p_h^k, \mathcal{P}_h w\big)_h + \xi\big(g\bar\nabla_h p_h^k, \bar\nabla_h \mathcal{P}_h w\big] = \frac{1}{\xi}\big(g f_0\big(p_h^k\big), \mathcal{P}_h w\big)_h + \xi\big(gF\big|\bar\nabla_h p_h^{k-1}\big|, \mathcal{P}_h w\big)_h.$$

Rewriting the preceding relation in terms of $\mathrm{L}_2(\Omega)$ and exploring the time-extension operators, we obtain

$$\begin{aligned}
&\xi\left(\frac{\partial \mathcal{Q}_\tau \mathcal{S}_h p_h^k}{\partial t}, \mathcal{S}_h\mathcal{P}_h w\right) + \xi\big(\mathcal{S}_h\mathcal{P}_h g \nabla \mathcal{S}_\tau \mathcal{Q}_h p_h^k, \nabla \mathcal{Q}_h \mathcal{P}_h w\big) - \xi \mathcal{S}_\tau E\big(p_h^k, p_h^k - \mathcal{P}_h p\big)\\
&\quad = \frac{1}{\xi}\big(\mathcal{S}_h\mathcal{P}_h g f_0\big(\mathcal{S}_\tau\mathcal{S}_h p_h^k\big), \mathcal{P}_h w\big) + \xi\big(\mathcal{S}_h\mathcal{P}_h(gF)\mathcal{S}_\tau\mathcal{S}_h\big(\big|\bar\nabla_h p_h^k\big|\big)(t-\tau), \mathcal{S}_h\mathcal{P}_h w\big).
\end{aligned} \tag{12}$$

We multiply (12) by a scalar function $\psi(t) \in \mathcal{C}^1(\langle 0,T\rangle)$, for which $\psi(T) = 0$. Integrating by parts, we arrive to

$$\begin{aligned}
&\xi\big(\mathcal{Q}_\tau\mathcal{S}_h p_h^0, \mathcal{S}_h\mathcal{P}_h w\big)\psi(0) - \xi\int_0^T \big(\mathcal{Q}_\tau\mathcal{S}_h p_h^k, \mathcal{S}_h\mathcal{P}_h w\big)\frac{\partial\psi}{\partial t}\,\mathrm{d}t\\
&\qquad + \xi\int_0^T \big(\mathcal{S}_h\mathcal{P}_h g\nabla\mathcal{Q}_h\mathcal{S}_\tau p_h^k, \nabla\mathcal{Q}_h\mathcal{P}_h w\big)\psi(t)\,\mathrm{d}t - \xi\int_0^T \mathcal{S}_\tau E\big(\mathcal{S}_h\mathcal{P}_h g p_h^k, p_h^k - \mathcal{P}_h p\big)\,\mathrm{d}t\\
&\quad = \frac{1}{\xi}\int_0^T \big(\mathcal{S}_h\mathcal{P}_h g f_0\big(\mathcal{S}_\tau\mathcal{S}_h p_h^k\big), \mathcal{P}_h w\big)\psi(t)\,\mathrm{d}t\\
&\qquad + \xi\int_0^T \big(\mathcal{S}_h\mathcal{P}_h(gF)\mathcal{S}_\tau\mathcal{S}_h\big(\big|\bar\nabla_h p_h^k\big|\big)(t-\tau), \mathcal{S}_h\mathcal{P}_h w\big)\psi(t)\,\mathrm{d}t.
\end{aligned}$$

We pass to the limit in all terms of this equation, knowing that $\mathcal{S}_h\mathcal{P}_h w \to w$, $\nabla\mathcal{Q}_h\mathcal{P}_h w \to \nabla w$, $\mathcal{S}_h\mathcal{P}_h g \to g$ and $\mathcal{S}_h\mathcal{P}_h(gF) \to gF$ uniformly in $\overline{\Omega}$, $\mathcal{S}_h\mathcal{P}_h p_{\mathrm{ini}} \to p_{\mathrm{ini}}$ as $p_{\mathrm{ini}} \in \mathcal{C}(\overline{\Omega})$, $\nabla\mathcal{S}_\tau\mathcal{Q}_h p_h^k \to \nabla p$ in $\mathrm{L}_2(0,T;\mathrm{L}_2(\Omega))$, $\mathcal{Q}_\tau\mathcal{S}_h p_h^k \to p$ in $\mathrm{L}_2(0,T;\mathrm{L}_2(\Omega))$, $f_0(\mathcal{S}_\tau\mathcal{S}_h p_h^k) \to f_0(p)$ in $\mathrm{L}_2(0,T;\mathrm{L}_2(\Omega))$ due

to the Aubin lemma (see also [6]), $\mathcal{S}_\tau\mathcal{S}_h|\bar{\nabla}_h p_h^k|(t-\tau) \to |\nabla p|$ in $\mathrm{L}_2(0,T;\mathrm{L}_2(\Omega))$ by Lemma 1, $\int_0^T \mathcal{S}_\tau E(p_h^k, p_h^k - \mathcal{P}_h p)\,\mathrm{d}t \to 0$ as $\nabla\mathcal{S}_\tau\mathcal{Q}_h p_h^k \to \nabla p$ in $\mathrm{L}_2(0,T;\mathrm{L}_2(\Omega))$, $\nabla\mathcal{S}_\tau\mathcal{Q}_h(p_h^k - \mathcal{P}_h p) \to \nabla p$ in $\mathrm{L}_2(0,T;\mathrm{L}_2(\Omega))$.

Taking into account all previous results, the fact that $\mathcal{S}_h p_h^0 = \mathcal{S}_h\mathcal{P}_h p_{\mathrm{ini}}$, and the Lebesgue theorem, we are able to pass to the limit.

$$\xi(p_{\mathrm{ini}}, w)\psi(0) - \xi\int_0^T (p, w)\frac{\partial\psi}{\partial t}\,\mathrm{d}t + \xi\int_0^T (g\nabla p, \nabla w)\,\mathrm{d}t = \frac{1}{\xi}\int_0^T \big(gf_0(p), w\big)\,\mathrm{d}t + \xi\int_0^T \big(gF|\nabla p|, w\big)\,\mathrm{d}t.$$

Obviously, the function p satisfies the initial condition in $\mathrm{L}_2(\Omega)$ (see [25]). The uniqueness shown in [6] allows to claim the convergence of the entire sequence of discrete solutions to the weak solution of the problem (6).

4. Numerical experiments

In this section, we present results obtained by means of the above-described algorithm. We process not only several artificially created examples, but we also test our approach on real photographically obtained images.

We first mention the nonlinear Gauss–Seidel iteration scheme for the resolution of (8), which represents a system of $(N_1-1)(N_2-1)$ nonlinear algebraic equations, and can be written as follows:

$$\xi\mathbf{A}\mathbf{p} - \frac{\tau}{\xi}\mathbf{f}(\mathbf{p}) = \xi\mathbf{F}, \tag{13}$$

where

$$\mathbf{p} = \big(p_{h,i,j}^k\big)_{i=1,j=1}^{N_1-1,N_2-1},$$
$$\mathbf{A}\mathbf{p} = \big(p_{h,i,j}^k - \tau\nabla_h\cdot\big(g\bar{\nabla}_h p_h^k\big)_{i,j}\big)_{i=1,j=1}^{N_1-1,N_2-1},$$
$$\mathbf{f}(\mathbf{p}) = \big(g_{i,j}f_0\big(p_{h,i,j}^k\big)\big)_{i=1,j=1}^{N_1-1,N_2-1},$$
$$\mathbf{F} = \big(p_{h,i,j}^{k-1} + \tau g_{i,j}F_{i,j}\big|\big(\bar{\nabla}_h p_h^{k-1}\big)_{i,j}\big|\big)_{i=1,j=1}^{N_1-1,N_2-1}.$$

We decompose the operator $\mathbf{A}$ using auxiliary operators

$$\mathbf{D}\mathbf{p} = \left(p_{h,i,j}^k + \tau\left(\frac{g_{i+1,j}+g_{i,j}}{h_1^2} + \frac{g_{i,j+1}+g_{i,j}}{h_2^2}\right)p_{h,i,j}^k\right)_{i=1,j=1}^{N_1-1,N_2-1},$$
$$\mathbf{L}\mathbf{p} = \left(-\tau\frac{g_{i,j}}{h_1^2}p_{h,i-1,j}^k - \tau\frac{g_{i,j}}{h_2^2}p_{h,i,j-1}^k\right)_{i=1,j=1}^{N_1-1,N_2-1},$$
$$\mathbf{U}\mathbf{p} = \left(-\tau\frac{g_{i+1,j}}{h_1^2}p_{h,i+1,j}^k - \tau\frac{g_{i,j+1}}{h_2^2}p_{h,i,j+1}^k\right)_{i=1,j=1}^{N_1-1,N_2-1},$$

so that we have $\mathbf{A} = \mathbf{D} + \mathbf{L} + \mathbf{U}$.

We solve (13) by means of the point-wise Gauss–Seidel nonlinear iterative method in the following form

$$\xi(\mathbf{D}+\mathbf{L})\big(\mathbf{p}^{l+1}-\mathbf{p}^{l}\big)=\xi\mathbf{F}-\left(\xi\mathbf{A}\mathbf{p}^{l}-\frac{\tau}{\xi}\mathbf{f}\big(\mathbf{p}^{l}\big)\right), \tag{14}$$

where the index l denotes the iteration sequence. For the initial guess, we choose the previous time level:

$$\mathbf{p}^{0}=\big(p_{h,i,j}^{k-1}\big)_{i=1,j=1}^{N_1-1,N_2-1}.$$

Remarks on the practical use of the scheme

In the segmentation tasks, the presented method exhibits behaviour similar to other level-set schemes and is semi-automatic, too, i.e., it requires an initial user's interaction. We give a recipe for the parameter values as follows:

(1) *Choice of F and p_{ini}*: Given the image P_0 to process, we choose the two parameters F and p_{ini} simultaneously by the usual experience with the behaviour of the mean-curvature flow in plane governed by the law

$$v_{\Gamma}=-\kappa_{\Gamma}-F, \tag{15}$$

where the closed curve Γ shrinks to a point when $F=0$, and this motion is accelerated for F positive, slowed, suppressed or even inverted for F negative. We either cover the objects of interest (a part of Ω, in which we expect to recognize some edges) by the set Ω_{ini} with the smooth boundary Γ_{ini} representing the initial segmentation curve and set $F>0$. Alternatively, we insert the set Ω_{ini} inside the object to be segmented, and set $F<0$. Then p_{ini} is the characteristic function of Ω_{ini}, or optionally its regularized version, and F can have the magnitude corresponding to $1/\operatorname{diam}\Omega_{\mathrm{ini}}$ and the sign mentioned above ensuring motion of Γ_{ini} by velocity of the order of $1/\operatorname{diam}\Omega_{\mathrm{ini}}$ (therefore not too slow, and not too fast) towards the edges of interest. The fine-tuning of the segmentation curve in the vicinity of the edge is performed by the terms containing the function g.

(2) *Choice of g*: The function g has the following form

$$g(s)=\frac{1}{1+\lambda s^2},$$

where $\lambda>0$ is a parameter. For $\lambda\in(5,50)$ used in our computations, we did not observe big difference in the result and in reliability of the method.

(3) *Choice of ξ, a, h and τ*: The parameter ξ relates the solution of (6) and the motion by mean curvature, as indicated in [3, Lemma 4.6]. However, we do not require any quantitative approximation of the mean-curvature flow by the Allen–Cahn equation (6), for the given range of applications. The extensive computational experience with the model (6) containing the gradient coupling term (see [4, 5] and compare with other computational results without such a term, e.g., in [24,19,30,15]) therefore suggests to take $\xi<0.1$ and $h\leqslant\xi$. The scheme (8) is proved to be unconditionally stable. However, the sufficient condition for the solvability of (8) suggests the relationship (11). The parameter a, which has no significant influence to the results, is set to $a=1$ in all experiments.

(4) *Choice of G_σ*: The function G_σ is represented by a 3×3 smoothing kernel. The convolution $G_\sigma * P_0$ can be computed beforehand.

(5) *Choice of the stopping time*: The time evolution generated by the algorithm for $k = 0, 1, \ldots$ is terminated whenever a position change of the recovery curve is below a specified threshold. For this purpose, we use the stopping criterion according to [37], i.e., we stop the computation as soon as the following inequality for the discrete values of the segmentation function holds

$$\frac{1}{M}\sum_{i,j}\left|p_{i,j}^{k+1} - p_{i,j}^{k}\right| \leqslant C\tau h^2. \tag{16}$$

The sum is over all grid points, M denotes the total number of grid points. The use of (16) originally developed for the level-set methods rely on the fact that the phase-field method works on a similar principle. This criterion is sometimes too strict, the solution p may not satisfy (16) yet, but the position of the interface is not visibly changing anymore.

In the following, we describe the computational experiments presented in Figs. 1–7. The parameters used for the computations are presented in the caption of each figure. During the evolution, a diffuse interface develops around the level line $p = 0.5$, which determines position of the segmentation curve. In the experiments with artificial images, we plot the segmentation function p from which the position of the curve is apparent. In the experiments with real images, we plot the recovery curve into the processed image P_0.

In Fig. 1, a shape recovery of four different objects in an artificial image (bottom right) is presented. The image was not degraded by noise. Sharp corners and quite a complicated shape of the letter 'R' are recovered. The solution p is shown at 5 subsequent time levels. Fig. 2 presents the same experiment performed on the image on which additive noise has been applied. The solution p is shown at 8 time levels. Apparently, the noise delays the curve evolution and therefore, the second experiment takes longer to stop. In Fig. 3, we present a numerical experiment on the artificial noisy image (bottom right) that was degraded by the "salt-and-pepper" noise. The results are shown at 5 time levels. Another experiment with the artificial image of the letter 'A' is presented in Fig. 4. Additive noise was applied to the image. We can see that a neighborhood of the letter is recovered very fast. However, most of the time evolution is spent in recovering the sharp corner in the upper part of the letter. The solution p is shown at 8 time levels. In the following experiments with real images, we do not plot the solution p, but only the position of the curve (i.e., the level set of p at 0.5). In Fig. 5, we present the experiment with an echocardiographic image. The initial position of the curve is given inside the human left ventricle. Due to the negative sign of F, the curve grows outwards. The curve is shown at 6 time levels. The original picture is provided by Prof. C. Lamberti, University of Bologna, Italy. The boundary at which the curve stops need not be very sharp as it is demonstrated in Fig. 6 of the satellite image of a tornado over the Indian Ocean. The curve is placed inside the cloud and expands outwards. In this experiment, a higher value of λ is used. The evolving curve is shown at 6 time levels. The original picture is provided by EUMETSAT (`http://www.eumetsat.de`). The last numerical experiment presented in Fig. 7 demonstrates the recovery of edges in the microscopic picture of a growing dendrite. The evolving curve is shown at 6 time levels. The original picture is provided with courtesy of H. Singer and J.H. Bilgram, Solid-State Physics Laboratory, Swiss Federal Institute of Technology Zurich, Switzerland (`http://www.dendrites.ethz.ch`).

Acknowledgements

The first author was partially supported by the project No. 201/01/0676 of the Grant Agency of the Czech Republic, the second author was partially supported by the project MSM98:210000010 of the Czech Ministry of Education, and the third author was partially supported by the project VEGA 1/0313/03. The authors also acknowledge partial support within the project No. 159 of the Czech–Slovak Science and Technology Programme.

References

[1] L. Alvarez, P.L. Lions, J.M. Morel, Image selective smoothing and edge detection by nonlinear diffusion II, SIAM J. Numer. Anal. 29 (1992) 845–866.
[2] G. Barles, H.M. Soner, P.E. Souganidis, Front propagation and phase field theory, SIAM J. Control Optim. 31 (1993) 439–469.
[3] M. Beneš, Mathematical analysis of phase-field equations with numerically efficient coupling terms, Interfaces and Free Boundaries 3 (2001) 201–221.
[4] M. Beneš, Mathematical and computational aspects of solidification of pure substances, Acta Math. Univ. Comenian. 70 (1) (2001) 123–152.
[5] M. Beneš, Diffuse-interface treatment of the anisotropic mean-curvature flow, Appl. Math. 48 (6) (2003) 437–453.
[6] M. Beneš, K. Mikula, Simulation of anisotropic motion by mean curvature–comparison of phase-field and sharp-interface approaches, Acta Math. Univ. Comenian. 67 (1) (1998) 17–42.
[7] S.C. Brenner, L.R. Scott, The Mathematical Theory of Finite Element Methods, Springer, New York, 1994.
[8] G. Caginalp, An analysis of a phase field model of a free boundary, Arch. Rational Mech. Anal. 92 (1986) 205–245.
[9] V. Caselles, R. Kimmel, G. Sapiro, Geodesic active contours, Internat. J. Comput. Vision 22 (1997) 61–79.
[10] F. Catté, P.L. Lions, J.M. Morel, T. Coll, Image selective smoothing and edge detection by nonlinear diffusion, SIAM J. Numer. Anal. 29 (1992) 182–193.
[11] Y.-G. Chen, Y. Giga, S. Goto, Uniqueness and existence of viscosity solutions of generalized mean curvature flow equations, J. Differential Geom. 33 (1991) 749–786.
[12] A. Handlovičová, K. Mikula, F. Sgallari, Semi-implicit complementary volume scheme for solving level-set like equations in image processing and curve evolution, Numer. Math. 93 (2003) 675–695.
[13] B.M. ter Haar Romeny (Ed.), Geometry Driven Diffusion in Computer Vision, Kluwer Academic, Dordrecht, 1994.
[14] R. Malladi (Ed.), Geometric Methods in Bio-Medical Image Processing, Springer, Berlin, 2002.
[15] C.M. Elliott, A.R. Gardiner. Double-obstacle phase-field computations of dendritic growth, Technical Report, CMAIA, University of Sussex, Brighton, 1996, Report No. 96/19.
[16] C.M. Elliott, M. Paolini, R. Schätzle, Interface estimates for the fully anisotropic Allen–Cahn equation and anisotropic mean curvature flow, Math. Models Methods Appl. Sci. 6 (1996) 1103–1118.
[17] L.C. Evans, H.M. Soner, P.E. Souganidis, Phase transitions and generalized motion by mean curvature, Comm. Pure Appl. Math. 45 (1992) 1097–1123.
[18] L.C. Evans, J. Spruck, Motion of level sets by mean curvature I, J. Differential Geom. 33 (1991) 635–681.
[19] X.B. Feng, A. Prohl, Numerical analysis of the Allen–Cahn equation and approximation for mean curvature flows, Numer. Math. 94 (1) (2003) 33–65.
[20] S. Fučík, A. Kufner, Nonlinear Differential Equations, TKI SNTL, Prague, 1978 (in Czech).
[21] J. Kačur, Method of Rothe in Evolution Equations, Teubner-Texte zur Mathematik, Teubner, Leipzig, 1985.
[22] J. Kačur, K. Mikula, Solution of nonlinear diffusion appearing in image smoothing and edge detection, Appl. Numer. Math. 17 (1995) 47–59.
[23] S. Kichenassamy, A. Kumar, P. Olver, A. Tannenbaum, A. Yezzi, Conformal curvature flows, Arch. Rational Mech. Anal. 134 (1996) 275–301.
[24] T. Kühn, Convergence of a fully discrete approximation for advected mean curvature flows, IMA J. Numer. Anal. 18 (1998) 595–634.

[25] J.L. Lions, Quelques Méthodes de Résolution des Problèmes aux Limites non Linéaires, Dunod, Gauthiers-Villars, Paris, 1969.
[26] R. Malladi, J. Sethian, B. Vemuri, Shape modeling with front propagation: a level set approach, IEEE Trans. Pattern Anal. Mach. Intel. 17 (1995) 158–174.
[27] K. Mikula, J. Kačur, Evolution of convex plane curves describing anisotropic motions of phase interfaces, SIAM J. Sci. Comput. 17 (1996) 1302–1327.
[28] R.H. Nochetto, M. Paolini, S. Rovida, C. Verdi, Variational approximation of the geometric motion of fronts, in: G. Buttazzo, A. Visintin (Eds.), Motion by Mean Curvature and Related Topics, de Gruyter, Berlin, 1994, pp. 124–149.
[29] S. Osher, R. Fedkiw, Levelset Methods and Dynamic Implicit Surface, Springer, Berlin, 2003.
[30] M. Paolini, An efficient algorithm for computing anisotropic evolution by mean curvature, in: J. Spruck, A. Damlamian, A. Visintin (Eds.), Curvature Flows and Related Topics, Gakkotosho, Tokyo, 1995.
[31] M. Paolini, C. Verdi, Asymptotic and numerical analyses of the mean curvature flow with a space-dependent relaxation parameter, Asymptotic Anal. 5 (1992) 553–574.
[32] P. Perona, J. Malik, Scale space and edge detection using anisotropic diffusion, IEEE Trans. Pattern Anal. Mach. Intell. 12 (1990) 629–639.
[33] A.A. Samarskii, Theory of Difference Schemes, Nauka, Moscow, 1977.
[34] A.A. Samarskii, Y.S. Nikolaev, Numerical Solution of Large Sparse Systems, Academia, Prague, 1984, Czech translation.
[35] J.A. Sethian, Level Set Methods, Cambridge University Press, New York, 1996.
[36] A. Visintin, Models of Phase Transitions, Birkhäuser, Boston, MA, 1996.
[37] H.K. Zhao, S. Osher, T. Chan, B. Merriman, A variational level set approach to multiphase motion, J. Comput. Phys. 127 (1996) 179–195.